CORONAL MAGNETOGRAPHY OF SOLAR ACTIVE REGION 8365 WITH THE SSRT AND NoRH RADIO HELIOGRAPHS

B. I. RYABOV
Institute of Astronomy, Latvian University, Riga LV-1586, Latvia

V. P. MAKSIMOV and S. V. LESOVOI
Institute of Solar-Terrestrial Physics, Irkutsk 664033, Russia

K. SHIBASAKI
Nobeyama Radio Observatory, Minamimaki, Nagano 384-13, Japan

A. NINDOS
Section of Astrogeophysics, Physics Department, University of Ioannina, Ioannina GR-45110, Greece

A. PEVTSOV
National Solar Observatory, Sacramento Peak, Sunspot, NM 88349, USA

Abstract. The microwave radio maps of solar active region NOAA 8365 are used to derive the coronal magnetograms of this region. The technique is based on the fact that the circular polarization of radio source is modified when microwaves pass through the coronal magnetic field transverse to the line of sight. The observations are taken with the Siberian Solar Radio Telescope (SSRT) on October 21 – 23 and with the Nobeyama Radio Heliograph (NoRH) on October 22 – 24, 1998. The known theory of wave mode coupling in quasi-transverse (QT) region is employed to evaluate the coronal magnetograms of 10 – 30 G at the wavelength 5.2 cm and 50 – 110 G at 1.76 cm, taking the product of electron density and the scale of coronal field divergence to be constant of 10^{18} cm^{-2}. The height of QT-region is estimated from the force-free field extrapolations as 6.3×10^9 cm for 20 G and 2.3×10^9 cm for 85 G levels. We find that on large spatial scale, the coronal magnetograms derived from the radio observations show similarity with the magnetic fields extrapolated from the photosphere.

1. Introduction

The ability to measure the strength of the magnetic field in the solar corona is of great value for the analyses of structural peculiarities in an active region magnetosphere. There are three polarization radio observation techniques best suited for magnetographic measurements: (1) the model reconstruction of observed gyro resonance emission introduced by Alissandrakis *et al*., 1980 and used by Brosius *et al*., 1997; (2) the observation of free-free emission proposed by Gelfreikh, 1999; and (3) the observation of the polarization inversion due to the quasi-transverse (QT-) propagation of microwave emission described by Ryabov *et al*., 1999 (hereafter Paper I). Our present paper deals with this third technique, which allows measure the strength of magnetic field transverse to the line of sight. Theoretically the quasi-transverse propagation of microwaves is well understood (Zheleznyakov, 1970).

Observationally one should detect the change of the circular polarization sign (inversion) in a source either at a given wavelength in time (Peterova and Akhmedov, 1974; Kundu and Alissandrakis, 1984; Maksimov and Bakunina, 1991; Alissandrakis *et al*., 1996) or using simultaneous observations at several wavelengths at a given time (Peterova and Akhmedov, 1974; Lee *et al*., 1998). In practice, however, all stages of the process of the coronal magnetography need further improvements, especially for the case of a weakly polarized microwave source.

In Paper I we have shown that a two-dimensional coronal magnetogram can be evaluated using radio observations with the Nobeyama Radio Heliograph at 1.76 cm, if the microwaves emitted by a bright strongly polarized source cross the overlying coronal fields at the right angle, and the field strength lies within 70 – 100 G. In this paper we focus on a wide weakly polarized microwave source of solar active region NOAA 8365, where the inversion of the circular polarization is traced both at a long (5.2 cm) and short (1.76 cm) wavelenghths. We use the radio observations from two instruments, the Siberian Solar Radio Telescope (SSRT) and the Nobeyama Radio Heliograph (NoRH) to evaluate a set of two-dimensional, 60″ – 120″ wide coronal magnetograms for fields in two ranges (10 – 30 G and 50 – 110 G). The low degree of circular polarization of the active region radio components complicates the analysis and introduces uncertainties. However, we are able to derive the coronal magnetograms about 3 times wider than in the case of the inversion in a bright sunspot-associated source treated in Paper I. We study the limitations of the coronal magnetography extended to a microwave source with a weak circular polarization.

2. Observations

The active region (AR) NOAA 8365 has emerged near central meridian at the latitude S28^{o} on October 19 and disappeared behind west limb on October 25, 1998. The region evolved rapidly during its disk passage. From October 19 to October 23, 1998 the sunspot area of the active region was doubling every day and it peaked at 360 millionth of solar hemisphere on October 23. The maximum strength of the photospheric magnetic field persisted at the level of 2200 – 2600 G for the preceding sunspot S1 of negative polarity and at 1900 – 2100 G for the following sunspots S2, S3 of the positive polarity (Figure 1a). The area decreased drastically to its initial level of 10 millionth of solar hemisphere during October 24 – 25. It should be noted that the rapid evolution of active region complicates the coronal magnetography. Nevertheless, we have selected this region for study because of good coverage of polarization inversion phenomenon by the Siberian Solar Radio Telescope and the Nobeyama Radio Heliograph. To calculate the wide-area coronal magnetograms we analyze a wide radio source observed by these two instruments.

In addition to the radio observations, we employ the photospheric vector magnetograms of AR NOAA 8365 taken with the Haleakala Stokes Polarimeter (HSP, Mickey 1985) of Mees Solar Observatory. The photospheric magnetograms are used to correlate the distribution of the magnetic field in photosphere and polarity of circular polarization in radio V maps taken with the SSRT at the wavelength of 5.2 cm and with the NoRH at 1.76 cm. Figures 1 – 3 show examples of our observations.

As the prevalence of extraordinary mode emission implies, the most of western microwave source A (Figures. 1d, 3a) is left circular (LC) polarized and the eastern source B is right circular (RC) polarized. As the active region moves toward the western limb, the source A changes its polarization to RC (Figures. 1f, 3c). The characteristic features of this reversal are discussed below.

2.1. POLARIZATION INVERSION AT 5.2 CM

The SSRT consists of 256 2.5m-diameter dishes forming a crossed interferometer with two arms of 622 m in length. RC and LC polarizations are recorded at the 5.2 cm wavelength (5.7 GHz) with the angular resolution of 21″ (Uralov *et al*., 1998; Grechnev *et al*., 1999). The telescope was used to produce 8 radio maps of the full solar disk daily. Each map was averaging of a set of 2 minutes maps of the Sun taken at one of the consecutive an hour periods on October 21 – 23.

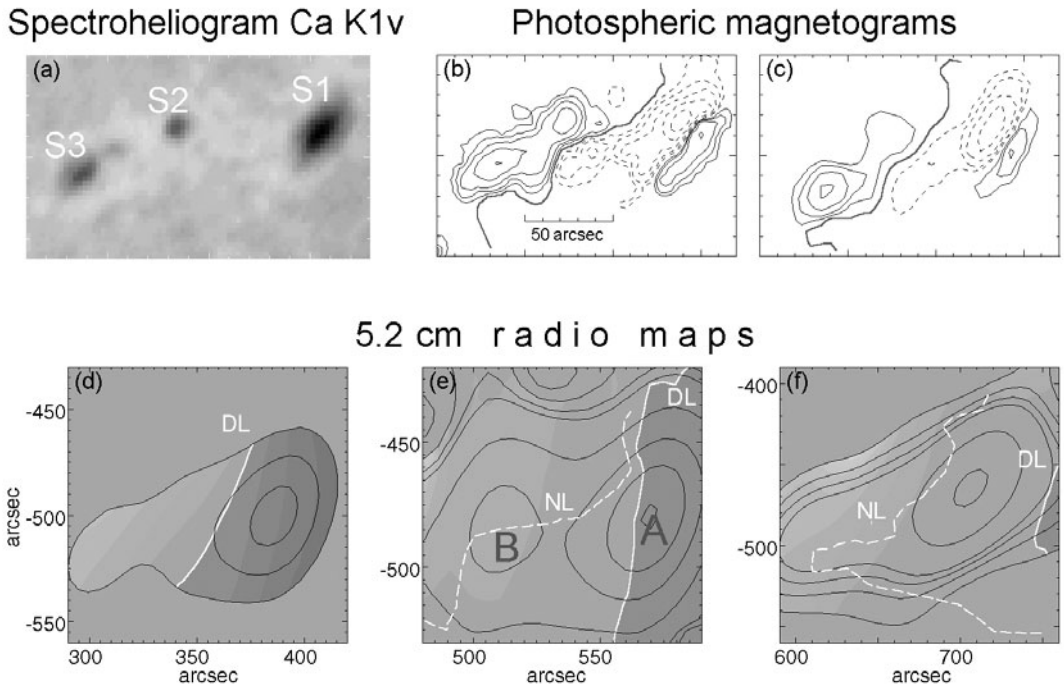

Figure 1. Active region NOAA 8365. *Upper row:* (a) Paris Observatory spectroheliogram Ca K1v, October 22, 13:09 UT. HSP observations: longitudinal magnetograms on (b) October 22, 21:23 UT and (c) October 23, 17:34 UT. *Lower row:* SSRT radio maps. The degree of circular polarization, $\rho^V = V/I$, observed on (d) October 21, 5:48 UT, (e) October 22, 5:54 UT, and (f) October 23, 3:36 UT. The brighter (darker) halftones represent RC (LC) polarization at [±0.1, ±0.2, ±0.3, ±0.4] levels. The black contours corresponds to total intensity I at [2, 4, 6, 8, 20, 40, 60, 80, 100] × 10^4 K with an outmost contour at 2 × 10^4 K. The degree of polarization is plotted only in the regions of significant local radio brightness (I > 2 10^4 K). The photospheric magnetic neutral line (NL, white dashed line) is smoothed and projected from HSP magnetograms. Note the westward displacements of the zero polarization V = 0 line (DL, white solid line) with time and more uniform distribution of circular polarization in active region on October 22 – 23 (panels e and f). North is up, and east is left.

To avoid artifacts we have calculated the degree of circular polarization for the region where the local radio brightness $I > 2 \times 10^4$ K. The errors in calculated degree of circular polarization are under 5 %. The western local source core (Figure 1) is only weakly polarized, $|\rho^V| = 3 - 10$ % at 5.2 cm, throughout the whole series of SSRT maps taken on October 22 – 23, 1998.

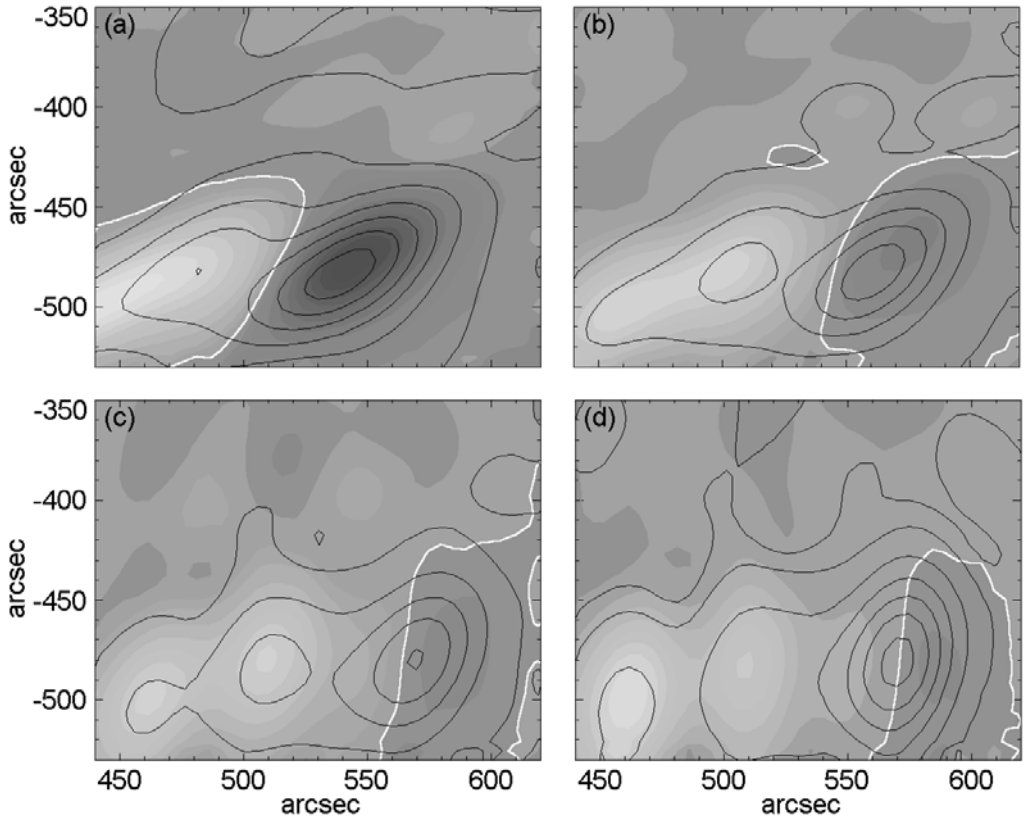

Figure 2. SSRT synthesis radio maps of AR 8365 in Stokes I (black contours) and V (grayscale) taken at 5.2 cm on October 22, 1998 at (a) 2:54 UT, (b) 3:54 UT, (c) 5:54 UT, and (d) 6:54 UT. Note the displacements of the depolarization line V = 0 (white solid line) above the western (right side) sunspot-associated microwave source. The contour levels of total intensity I are $[5, 20, 40, 60, 80, 100, 120] \times 10^4$ K. Bright halftones represents the right-hand circular polarization and dark corresponds to the left-hand circular polarization. V contour levels are $[5, 10, 20, 30, 40, 50, 60, 70, 80, 90, 100] \times 10^3$ K.

The shape of the depolarization line (DL) V = 0 changes during the observations, however DL moves progressively towards the western solar limb during October 22 – 23 (Figures 1 d – f). Some short-term deviations from the progressive westward movement are perceived in a few pairs of the adjacent V maps. Noteworthy is also the low degree of circular polarization $\rho_A^V = -7\%$ of the source A on October 22 as compared with the averaged degree of about – 25% on October 21. Both the eastern source B and western source A have approximately equal (but opposite in sign) polarization on October 21. However, the western source A is about 3 times less

polarized in the first map taken on October 22. The source B looks extended and rather close to the photospheric magnetic neutral line (NL), B_l =0. It is evident that the radiation of the source A is affected by QT-propagation during the whole period of the SSRT observations on October 22.

2.2. POLARIZATION INVERSION AT 1.76 CM

The NoRH is a radio interferometer comprised of 84 80 cm-diameter dishes arranged in a T-shaped array. The array is 490 m in length in the east-west direction and 220 m in north-south direction and it provides a spatial resolution of 10″ and a temporal resolution of 1s. Both RC and LC polarizations are recorded at the wavelength of 1.76 cm (17 GHz). The circular polarization of about 1% is detectable (Nishio *et al*., 1994; Hanaoka *et al*., 1994).

The NoRH images in Stokes I and V were processed using aperture synthesis techniques. One-hour long visibility data sets were imported into AIPS and treated with the method described by Nindos *et al*. (1999). The maximum entropy method (MEM) was used for the deconvolution of the dirty maps after the bright sources were CLEANed out. Before adding back the CLEAN components of the bright emission we rotated them to a common time which was the middle of the visibility data set (see Nindos *et al*., 2000). Our final maps have spatial resolution of about 14″. In order to better delineate the DLs each resulting map was averaged over 26″. Doing so we miss small-scale features of about 10″ – 26″ but such fine structures are not crucial for the subsequent analysis.

Figure 3 shows the example of NoRH observations. To avoid artifacts we have studied the degree of circular polarization for the region where the local radio brightness $I > 2 \times 10^4$ K. The polarization inversion at 1.76 cm in NOAA 8365 is first detected on October 23, 1998 (peak value of the degree of the source A is ρ_A^V = – 3%). While the sign of circular polarization has inverted on October 24 (ρ_A^V = + 4%), the absolute value is not as high as on October 22 (ρ_A^V = – 23%).

The time-period and wavelength dependences of the inversion listed by Peterova and Akhmedov (1974) are in good agreement with expected QT-propagation for the western core radiation:

1. Due to the strong dependence of QT-propagation on frequency (see Section 3.1) one expects that the closer an AR to the western solar limb is, the shorter is an operational wavelength required to detect the inversion.
2. DL moves toward the western solar limb while the polarization inversion is observed at a fixed wavelength.
3. The post-inversion value of the degree of circular polarization, as a rule, does not exceed the pre-inversion one.

Thus both the SSRT (Figure 1) and the NoRH observations (Figure 3) indicate the polarization inversion due to QT-propagation. Spectral polarization radio observations of AR 8365 made with the RATAN-600 support that (Ryabov and Maksimov, 1999).

It is clear, that the circular polarization was reversed not only in the sunspot-associated source A, but over the western plage as well. This is important evidence in

respect to the coronal magnetography. Whether this effect can be exploited for coronal magnetography will be discussed in Section 5.

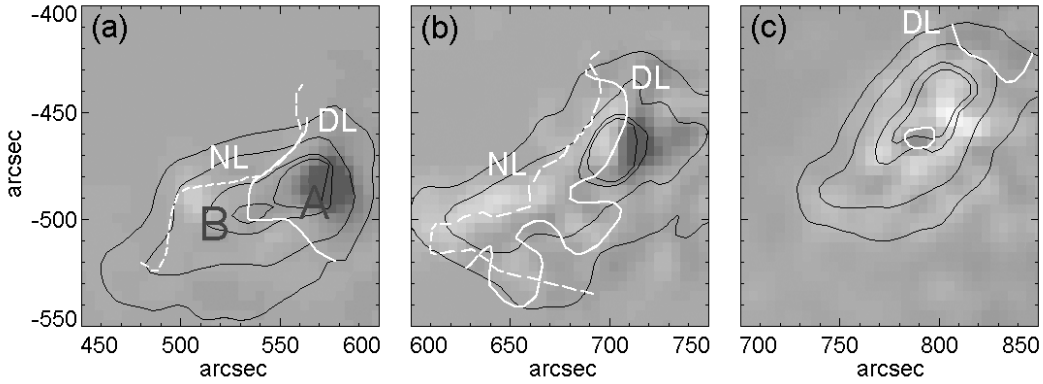

Figure 3. Radio maps in Stokes I (black contours) and the degree of circular polarization V/I (grayscale) taken with the NoRH at $\lambda = 1.76$ cm on (a) October 22 (6:00 UT), (b) October 23 (5:00 UT), and (c) October 24 (6:00 UT). The contour levels of total intensity I are [2, 4, 8, 10] $\times 10^4$ K with an outmost contour at 2×10^4 K. RC (bright halftones) and LC (dark halftones) polarization are separated by the depolarization line (DL, white solid line). V halftones are not drawn to one scale through the panels (a) – (c).

To make a rough estimate of DL's shift in image plane we removed the solar rotation and disregarded the variations of the non-progressive movement of DL. The DL shift is found to be 48″ per day at 5.2 cm (at the longitudinal displacement $\theta = 40^o$ from central solar meridian) and 32″ per day at 1.76 cm ($\theta = 52^o$).

3. Coronal magnetograms

3.1. TECHNIQUE OF CORONAL MAGNETOGRAPHY

The technique of coronal magnetography through QT-propagation of microwaves is described in Paper I and is only briefly discussed here.

Let a sunspot-associated microwave source emit radiation with circular polarization ρ^V_0. If the radiation passes through QT-region (QTR, area where the magnetic field is nearly perpendicular to the line-of-sight), the sign and the degree ρ^V of the resulted circular polarization depends mainly on the strength B of the transverse magnetic field in the QTR. This allows evaluate the coronal magnetic fields, provided the electron density N and the scale of the magnetic field divergence L_α in QTR are known. The relation between the initial polarization ρ^V_0 before passing a QTR and the observed ρ^V is derived by Zheleznyakov and Zlotnik, 1964:

$$\rho^V = \rho^V_0 \, [2 \exp(-2\delta_0) - 1]. \qquad (1)$$

The quantity $2\delta_0$ is related with the parameter of electromagnetic wave coupling in QTR (Cohen, 1960; Zheleznyakov, 1970; Bandiera, 1982).

$$2\,\delta_0 \approx 1.15 \times 10^{-25}\, B^3\, N\, L_\alpha\, \lambda^4, \qquad (2)$$

where λ is the operational wavelength of radio observations (all units are in c.g.s.). The magnetic field divergence $L_\alpha = \alpha_p \left\| \frac{d\,\alpha_p}{d\mathbf{l}} \right\|^{-1}$ varies as the reciprocal of the gradient of propagation angle α_p (the angle between the direction of electromagnetic wave propagation **l** and the ambient magnetic field **B**), since $\alpha_p \approx \pi/2$ in QTR.

If we define the normalized polarization as $P = \rho^V / \rho^V{}_0$ and assume constant value for $N\,L_\alpha = 10^{18}$ cm^{-2} (see Paper I for some reasoning), we get the magnetic field B in QTR from Equations (1), (2):

$$B \approx -2.05 \times 10^2\, \lambda^{-4/3}\, \ln^{1/3}(0.5\,P + 0.5). \qquad (3)$$

When the source is near the solar disk center, the radio waves cross QTR higher up in the corona, where the magnetic field B is weak and the resulting polarization ρ is the same as in front of the QTR, that is ρ_0. As the source moves towards the limb the radiation crosses QTR lower in the corona and when the region is at particular distance from the disk center, the sign of resulting circular polarization (due QTR) reverses. The technique is most sensitive to the strength of B corresponding to $\rho^V \approx 0$. More precisely, the highest sensitivity of the measurements corresponds to

$$\rho^V = \rho^V{}_0\,[2\exp(-2/3) - 1] \approx 2.68 \times 10^{-2}\,\rho^V{}_0. \qquad (4)$$

To verify this estimate the equation $\frac{\partial^2 \rho^V}{\partial^2 B} = 0$, implying the maximum of the function $\left|\frac{\partial \rho^V}{\partial B}\right|$, should be derived.

Thus, the radio observations at operational wavelength λ (in cm) are most responsive to the magnetic field B (in G) in the QTR defined as

$$B \approx 180\,\lambda^{-4/3}. \qquad (5)$$

For example, the SSRT (5.2 cm) and the NoRH (1.76 cm) are most sensitive to the coronal fields of 20 G and 85 G accordingly, provided that $N\,L_\alpha = 10^{18}$ cm^{-2}.

To make the most of the Equation (3), the full range (–1, +1) of the normalized degree of circular polarization $\rho^V/\rho^V{}_0 = P$ can be used (Paper I). As a result, not only the coronal field responsible for zero circular polarization, but the entire 2D coronal magnetogram may be evaluated. Let the borders of the coronal magnetograms be defined by $|P| \le 1 - \sigma$. The value of σ determines the relative accuracy of ρ^V maps. In case of SSRT observations $\sigma = 0.05$, and for NoRH data $\sigma = 0.01$. The reasonable limitation of $|P| \le 0.95$ is used throughout this paper, which implies the strength of magnetic fields derived from the radio measurements to be 6.7 – 35 G at 5.2 cm and

28 – 150 G at 1.76 cm. The normalized degree of circular polarization P is sensitive to the QT-propagation alone and quite insensitive to the emission mechanism. Thus, a coronal magnetogram in image plane will be determined only by the magnetic field in coronal QTR, which "screens" the microwave source.

The computation procedure usually starts with the selection of a map ρ^{V}_{0} = V/I suitable for the normalization. The map is considered to be suitable for normalization if there is no evidence of polarization inversion at the operational wavelength in the region. E.g., a bipolar active region situated near the center of solar disk appears as a bipolar microwave source if no polarization inversion occurs. The next step is to shift the sampled ρ^{V} maps to the normalization map ρ^{V}_{0} position on solar disk. The position tends to be near the central solar meridian. The position of maximum in total intensity I would be brought into coincidence with the maximum of normalization map. A set of sampled maps covers the overall process of polarization inversion, that is, from the beginning, when the polarization of a source with the initial polarization sign is only slightly suppressed, to the end, when the polarization of a source with the inverted sign attains its maximum value. Finally, the normalized P maps are converted into coronal magnetograms using Equation (3).

3.2. CORONAL MAGNETOGRAMS

The coronal magnetograms obtained show the features intrinsic to the magnetic field distribution in the QTR projected to the image plane. We will specify some distinct features to prove the magnetographic nature of normalized radio maps P. Our discussion will also focus on the QT-surface ($\alpha_p = \pi/2$) because it is a significant geometrical feature. It presents a large-scale outline of active region magnetosphere, if the direction of the line of sight is taken into consideration.

(1) Since the photospheric neutral line (NL) is a lower border of QT-surface, it is evident that the projection of the strong coronal field to image plane should be closer to the neutral line than that of the weak coronal field. This is true as far as the wavelength of radio observations is concerned: the shorter the wavelength is, the closer the depolarization line lies to the neutral line (cf. DL and NL in Figures 1e and 1f with Figures 3a and 3b).

(2) The depolarization line, as well as any line where P = *constant* in image plane, tends to move toward the western solar limb during the polarization inversion (Figure 3; Figures 4, 5c).

(3) The gradient of the coronal magnetic field strength is in west-east direction for a bipolar active region situated in western hemisphere (Figures 4 and 5). The distribution is shaped through the intersection of isogaussian surfaces by QT-surface. Hence, progressive smoothing is observed with the wavelength increase.

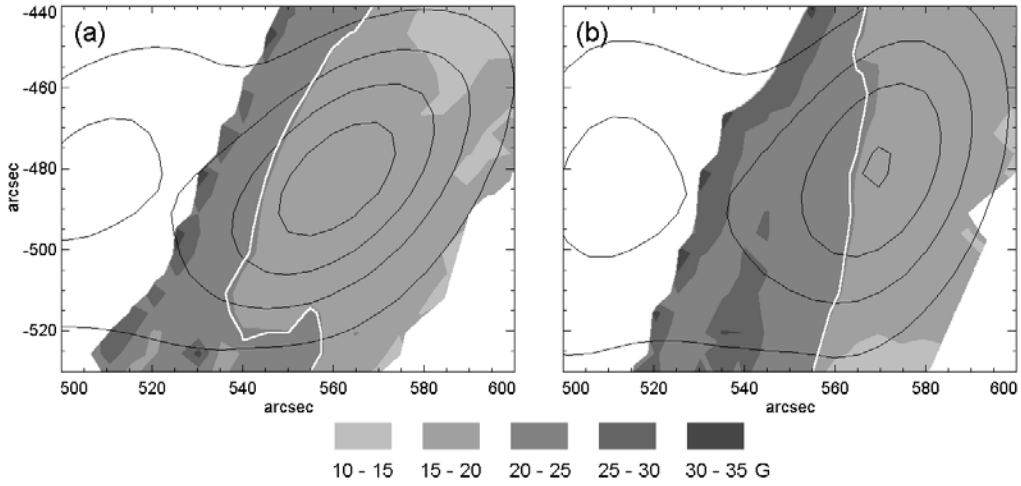

Figure 4. Two coronal magnetograms are overlaid on the contours of the total radio brightness at 5.2 cm in image plane. The halftones corresponding to the coronal magnetic fields 10 – 15, 15 – 20, 20 – 25, and 25 – 30 G are clearly seen. The normalizing degree of circular polarization is calculated as V/I SSRT radio map taken at 2:54 UT, while the coronal magnetograms result from V/I maps taken in the polarization inversion course at (a) 3:54 UT and (b) 5:54 UT, normalized by the V/I map of October 22 and referred to the position of the normalizing map. The depolarization line is marked by the white line.

It should be noted that in spite of a weak radio brightness of the polarized source A, the intrinsic features of coronal magnetogram are clearly seen in Figure 4 (SSRT observations). The range of magnetic field in this magnetogram is 10 – 30 G. Figures 5 a and b show coronal magnetograms derived using NoRH observations. Compared with P contours on October 22, 1998 (Figure 4), the contours on October 23 (Figure 5c) appear to be more "curved" in accordance with lower coronal heights.

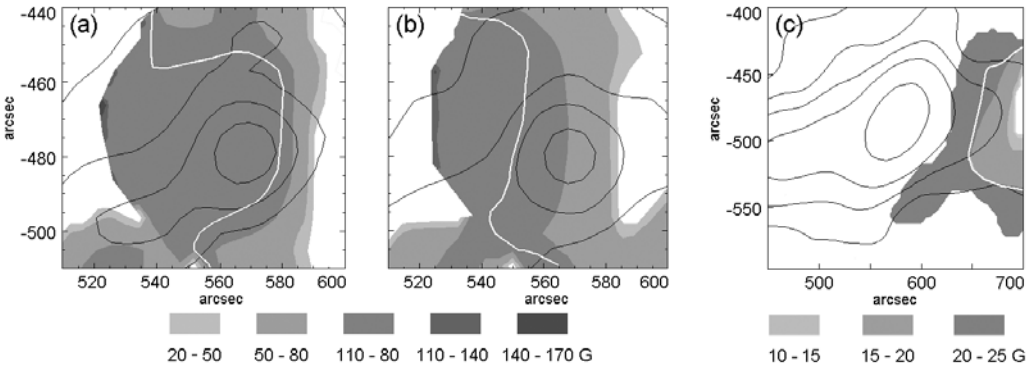

Figure 5. Coronal magnetograms: (a) and (b) are overlaid on the contours of radio brightness at 1.76 cm in the image plane. The normalizing degree of circular polarization is calculated as the V/I NoRH radio map of October 22 6:00 UT, while the coronal magnetograms result from the V/I maps taken in the polarization inversion course at (a) 2:55 UT and (b) 5:00 UT October 23, normalized by the V/I map of October 22 and referred to the position of the normalizing map. A coronal magnetogram (c) is overlaid on the contours of the radio brightness at 5.2 cm in the image plane. The normalizing degree of circular polarization is calculated as the V/I SSRT radio map taken on October 22 at 2:54 UT, while the coronal

magnetogram results from the V/I map taken in the polarization inversion course on October 23 at 4:36 UT, normalized by the V/I map of October 22 and referred to the position of the normalizing map. The depolarization line is marked by the white line.

The range of clearly seen values in the NoRH magnetograms is 50 – 110 G. The coronal magnetograms of 50 – 110 G isogauss observed with the NoRH (Figures 5a, 5b) are consistent with the 10 – 30 G magnetogram measured with the SSRT on October 23 (Figure 5c). As expected, the coronal field distribution resulting from NoRH maps differs from the distribution from SSRT maps in the sense that it delineates clearer the location of the sunspot S1. The coronal field gradient is estimated to be 3×10^{-9} G cm^{-1} in respect to image plane and it is referred to the coronal height of 7×10^9 cm in agreement with estimates by Gelfreikh *et al*. (1996).

In the presence of active region evolution, the coronal magnetograms with long time interval between ρ^V and $\rho^V{}_0$ radio maps will be the subject of greater uncertainty. Hence, the observed evolution of the AR 8365 leads us to expect that the coronal magnetograms in Figure 4 (1 – 3 hour interval) are more reliable than those of Figure 5 (21 – 26 hour interval). There seems to be a limiting case of a faint circularly polarized source that makes the coronal magnetography feasible.

4. Model analysis

4.1. QTR HEIGHTS

It is evident that geometrically, the higher (in QTR) the isogaussian producing the total depolarization is, the faster its projection (DL) moves in image plane and the faster the polarization inversion proceeds. Generally, any P = *constant* line of the normalized radio polarization can be used for the height estimation. In a framework of fixed QTR approach (Gelfreikh *et al*., 1987) the averaged rate of inversion at 5.2 cm (DL moves 2″ per hour across the microwave source on October 22, 1998) results in the coronal height of 1.4×10^{10} cm for the field strength of 20 G. Alternatively, the height of the magnetic field in QTR can also be evaluated using the horizontal dipole approximation (Bandiera, 1982; Kundu and Alissandrakis, 1984; Alissandrakis, 1999). Using the distance between NL and DL we calculated the heights corresponding to 20 G contour following Kundu and Alissandrakis (1984). For October 22 observations this method yields a height of 1.2×10^{10} cm. Finally, Ryabov and Maksimov (1999) used the superposition of 5 dipoles to simulate the polarization inversion at 5.2 cm in the AR 8365. They found a height of 7×10^9 cm for the coronal field of 20 G.

4.2. MAGNETIC FIELD EXTRAPOLATION

The photospheric magnetic field extrapolated into the corona can be used to simulate the QT-surface and to estimate the heights of magnetic fields with a particular field strength. To test the relationship between the radio measurements presented in Section 3.2 and the magnetic field extrapolated from photosphere we computed two

models, i.e., potential field (PF: $\nabla \cdot \mathbf{B} = 0$, $\nabla \times \mathbf{B} = 0$) and linear force-free field (FFF: $\nabla \times \mathbf{B} = \alpha_{fff} \mathbf{B}$). The extrapolation was done using HSP vector magnetograms.

The QT-surface calculated from PF model (not shown) partly covers the source A overlying the sunspot S1 with the coronal fields B < 20 G. It is insufficient to invert the sign of circular polarization at 5.2 cm and hence we conclude that PF extrapolation does not properly represent coronal field of this active region. This finding is in agreement with previous studies. For example, Lee *et al*. (1999) correlated the temperature maps observed by VLA at 6.2 cm (4.9 GHz) and 3.5 cm (8.4 GHz) and used potential and nonlinear force-free field extrapolations to construct the field lines connecting these two surfaces. They found that potential model does not adequately represent the coronal fields in areas with high shear (non-zero electric currents).

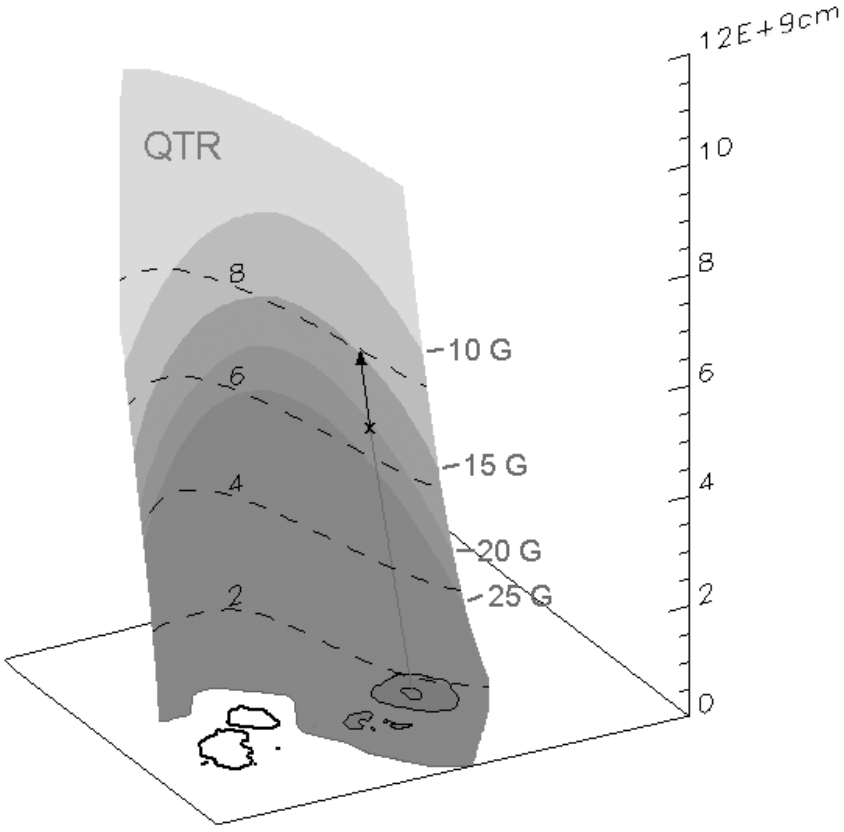

Figure 6. Calculated 3D QT-surface in the AR 8365 on October 22, 1998. The surface, where propagation angle $\alpha_p = 90°$, is calculated with PF extrapolation on the base of the HSP vector magnetogram. The rendered region of the QT- surface is cut at the heights 8×10^8 cm and 1.2×10^{10} cm. The dashed lines mark the heights of surface horizontal sections in the units of 10^9 cm. The halftones represent the coronal magnetic field strength of 5 G < B ≤ 25 G in the QTR. The ray path (an arrow) from the preceding sunspot crosses the QTR at the height of 6×10^9 cm (a cross), the coronal fields of 20 G just appropriate to depolarize the

circular polarization at 5.2 cm. The circular polarization sign at 5.2 cm reverses depending on whether microwaves cross the QT-surface lower (inverted sign) or higher the isogaussian 20 G (preserved sign).

Next we computed linear FFF model. Constant $\alpha_{fff} = 4.9 \times 10^{-11}$ cm^{-1} was determined as in Pevtsov *et al*. (1995) by minimizing a difference between computed and observed horizontal fields. The model with this α_{fff} was found to produce the field strengths just enough to simulate the polarization inversion at 5.2 cm (Figures 6 and 7).

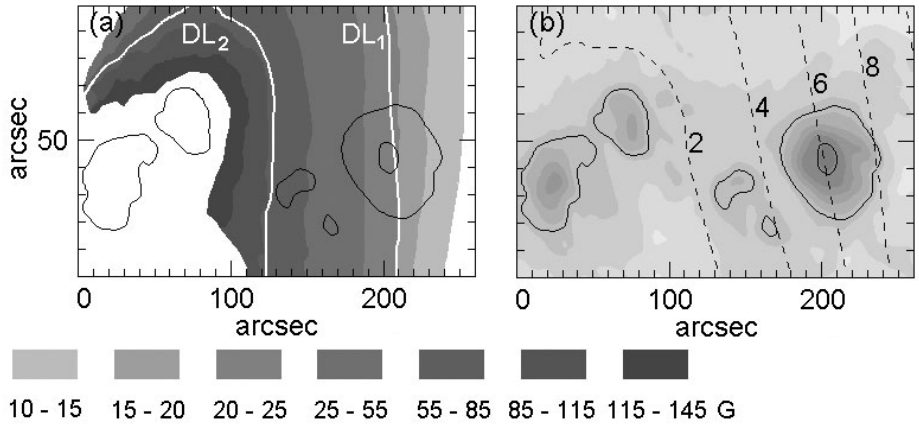

Figure 7. The coronal magnetic field strength on the QT-surface (a) and the horizontal section heights through the QT-surface (b) projected to the image plane. The FFF extrapolation with $\alpha_{fff} = 4.9 \times 10^{-11}$ cm^{-1} on the base of the HSP magnetogram taken on October 22, 1998. The contours of coronal field (a) and the contours of the coronal height of the QT-surface [2, 4, 6, 8] $\times 10^9$ cm (b) are projected on the photospheric tangential plane. The major sunspots are delineated by 515 G and 1520 G contours (4th harmonic of electron gyrofrequency of 5.7 GHz and 17 GHz). The white lines marked DL_1 and DL_2 represent the depolarization lines at 5.2 cm and 1.76 cm correspondingly.

Comparing the model's depolarization line DL_1, derived from FFF extrapolation (Figure 7a) with the observed one in the vicinity of the microwave source A at 5.2 cm (Figure 1e), a similarity can be found. The DL_2 position corresponds with the depolarization line position observed at 1.76 cm (Figure 3a). As for the shape, the observed depolarization contours vary, especially at 1.76 cm, in the case of this active region. The depolarization line DL_2 simulated at 1.76 cm (taking into account the model values of electron density N and the scale L_α) is close but it does not completely coincide with the projection of 85 G isogaussian. This line is somewhat higher than the 85 G in its northern part because the value of N L_α varies with height (see Equation 2).

The model field distribution in image plane is somewhat smoother than the observed coronal magnetogram (cf. Figure 4b and Figure 7a). Some details in the model distribution, such as the "kink", do not coincide with the corresponding

features in coronal magnetograms. However, we note the structural similarity between observations and FFF model on large spatial scale, namely, the direction and the characteristic value of the magnetic field gradient. This similarity validates the coronal magnetography technique used here.

The heights of the magnetic fields involved in the polarization inversion resulting from the FFF approximation depend on the value of the constant α_{fff}. The FFF model with $\alpha_{fff} = 4.9 \times 10^{-11}$ cm^{-1} leads to the coronal heights of $(5 - 9) \times 10^9$ cm for the magnetic fields of 30 – 10 G and $(1.5 - 3.8) \times 10^9$ cm for the fields of 110 – 50 G. These heights are in agreement with 5 dipoles superposition, but it is slightly lower than the heights estimated using fixed QTR approach method (see Section 4.1). On the other hand, potential field approximation yields heights that are significantly lower than 6.2×10^9 cm (20 G) and 2.3×10^9 cm (85 G) from the FFF approximation.

Lee *et al*. (1998) have noted that the inclination of QT-surface to photosphere rather than the QTR height may be the crucial parameter as the polarization inversion rate is concerned (see also Alissandrakis *et al*., 1996). The parameter α_{fff} of FFF approximation governs the inclination and, thus, the position of DL projection. This might complicate the seemingly simple task of the evaluation of coronal height from a set of DLs projected from the QTR.

5. Summary and Conclusions

We have investigated the polarization inversion phenomenon observed with the SSRT and the NoRH radio heliographs in wide $60'' \times 60''$ area above NOAA 8365. We have observed the polarization inversion, which is due to the QT-propagation of microwaves in solar corona above this active region. The evidence of QT-propagation is present in time and wavelength dependence of polarization inversion observed in 1D radio scans taken with RATAN-600 (Ryabov and Maksimov, 1999) and in 2D maps observed by the SSRT and the NoRH. Using the radio maps from two radio heliographs we derived 2D coronal magnetograms corresponding to 30 – 10 G at the coronal height of about $(5 - 9) \times 10^9$ cm and 110 – 50 G at the heights of $(1.5 - 3.8) \times 10^9$ cm. The magnetograms are derived under the assumption that the product of electron density and the coronal field divergence scale is 10^{18} cm^{-2}. The coronal magnetograms are considered to be the subjects for further refinements when more precise electron density and the scale values become available.

Our attempt of coronal magnetography of a faint and evolving active region has encountered a difficulty. Namely, the depolarization line (DL) is not stable in shape. It is moving progressively limbward in course of polarization inversion. One might expect such westward movement of the DL as the Sun rotates. As the result of change in the position angle of the region, the QT-surface is crossed by microwaves lower and lower in the corona. However, we found that successive V maps at 1.76 cm do not reproduce the shape of DL from one map to the other. Furthermore, some additional displacements of DL in the SSRT maps observed at 5.2 cm are superimposed on the progressive westward movement of DL. In part, this may be due to rapid evolution of the active region.

The NoRH data have an intrinsic uncertainty of about 14″ and the self-calibration steps applied to the radio data to improve the images can introduce further uncertainty. However, we note that we have overlayed the synthesized NoRH images to nearly simulataneous SXT images using the known pointing of the instruments and the overlays are satisfactory (i.e. the extended thermal radio emission matches well the extended thermal soft X-ray emission).

The coronal magnetograms derived using these averaged radio maps reproduce the general features of the coronal magnetic fields extrapolated in FFF model from the photosphere.

The accuracy of our method of coronal magnetography is limited by accuracy of radio polarization measurements. In addition, the non QT-propagation effects may affect the normalization procedure. For example, in case of thermal microwave source at the top of a coronal loop, the line V = 0 corresponds to the coronal neutral line ($B_l = 0$) in image plane. If the microwaves from this thermal source cross QT-surface on the way to the observer, the radiation and propagation effects may be combined to form a modified DL (Alissandrakis and Preka-Papadema, 1984; Alissandrakis *et al*., 1993). Thus, in spite of radiation mechanism independence, the coronal magnetography using QT-propagation method should be conducted with a caution to insure that there are no non-QT distortions of the sampled V maps. In case of AR 8365 one can see the local intensity maximum A (Figures 1e, 3a) associated with a leg of coronal loops. Hence, we believe that the western microwave source A of the AR 8365 is stable at 1.76 cm and 5.2 cm in the projection DL sense and that our method of coronal magnetography is appropriate.

The rapid evolution of active region complicates the resulting radio magnetograms. One might expect that in slowly evolving bipolar regions the microwave polarization will vary only gradually over several days due to QT-propagation. Such regions will be more suitable for our method of coronal magnetography (Bezrukov *et al*., 2003).

Acknowledgements.

This work has been supported by INTAS grants Open Call 2000 00-0181 and 00-0543. One of the coauthors (B.I.R.) is grateful to Prof. D. Dravins from the Onsala Space Observatory for granting an IDL 5.3 package. He appreciates the hospitality and help of the Nobeyama Solar Group during his stay at the Nobeyama Radio Observatory. National Solar Observatory (NSO) is operated by the Association of Universities for Research in Astronomy Inc. (AURA) under cooperative agreement with the National Science Foundation.

References

Alissandrakis, C.E.: 1999, *Proc. of Nobeyama Symp.,* NRO Report **479**, 53.

Alissandrakis, C.E., Borgioli, F., Chiuderi Drago, F., Hagyard, M., Shibasaki, K.: 1996, So*lar Phys.,* **167**, 167.

Alissandrakis, C.E.,Kundu, M.R., Lantos P.: 1980, *Astron. Astrophys*., **82**, 30.

Alissandrakis, C.E., Nindos, A., Kundu, M.R.: 1993, *Solar Phys*., **147**, 343.

Alissandrakis, C.E. and Preka-Papadema, P.: 1984, *Astron. Astrophys*., **139**, 507.

Bandiera, R.: 1982, *Astrophys.J.,* **112**, 52.
Bezrukov, D.A., Grechnev, V.V., Ryabov, B.I.: 2003, *Baltic Astronomy*, (submitted).
Brosius, J.W., Davila, J.M., Thomas, R.J., White, S.M.: 1997, *Astrophys. J.,* **488**, 488.
Cohen, M.H.: 1960, *Astrophys. J.,* **131**, 664.
Gelfreikh, G.B.: 1999, *Proc. of Nobeyama Symp.,* NRO Report **479**, 41.
Gelfreikh, G.B., Peterova, N.G., Ryabov, B.I.: 1987, So*lar Phys.,* **108**, 89.
Gelfreikh, G.B., Pilyeva, N.A., Ryabov, B.I.: 1996, So*lar Phys.,* **170**, 253.
Grechnev, V.V., Altyntsev, A.T., Konovalov, S.K., Lesovoi, S.V.: 1999, in *Conf. Ser.- Astronomical Data Analysis Software and Systems VIII, eds. D.M. Mehringer, R.L. Plante, D.A. Roberts, San Francisco, ASP*, **172**, 329.
Hanaoka, Y., Shibasaki, K., Nishio, M., Enome, S., Nakajima, H., Takano, T., Torii, C., Sekiguchi, H., Bushimata, T., Kawashima, S., Shinohara, N., Irimajiri, Y., Koshiishi, H., Kosugi, T., Shiomi, Y., Sawa, M., Kai, K.: 1994, NRO, *Proc. of Kofu Symposium*, NRO Report **360**, 35.
Kundu, M.R. and Alissandrakis, C.E.: 1984, *Solar Phys*., **94**, 249.
Lee, J., White, S.M., Kundu, M.R., Mikic, Z., McClymont, A.N.: 1998, *Solar Phys.,* **180**, 193.
Lee, J. White, S.M., Kundu, M.R., Mikic, Z., McClymont, A.N: 1999, *Astrophys. J.,* **510**, 413.
Maksimov, V.P. and Bakunina, I.A.: 1991, *Soviet Astron.,* **35**, 194.
Mickey, D.L.: 1985, *Solar Phys*., **97**, 223.
Nindos, A., Kundu, M.R., White, S.M., Gary, D.E., Shibasaki, K., Dere, K.P.: 1999, *Astrophys.J*., **527**, 415.
Nindos, A., Kundu, M.R., White, S.M., Shibasaki, K., Gopalswamy, N.: 2000, *Astrophys.J., (Suppl.),* **130**, 485.
Nishio, M., Nakajima, H., Enome, S., Shibasaki, K., Takano, T., Hanaoka, Y., Torii, C., Shiomi, Y., Sekiguchi, H., Bushimata, T., Kawashima, S., Shinohara, N., Koshiishi, H., Kosugi, T., Sawa, M., Kai, K., Irimajiri, Y., Nohmi, H., Honda, K., Shinohara, H., Ito, T., Miyawaki, M., Imoto, A., Takabayashi, T., Nishikawa, K., Futagawa, N., Tanaka, S., Morikawa, H., Kitahara, Y., Harakawa, K., Mishima, K.: 1994, *Proc. of Kofu Symposium*, NRO Report **360**, 19.
Peterova, N.G., Akhmedov, Sh.B.: 1974, *Soviet Astron.,* **17**, 768.
Pevtsov, A.A., Canfield, R.C., Metcalf, T. R: 1995, *Astrophys. J.,* **440**, L109.
Ryabov, B.I. and Maksimov, V.P.: 1999, Proceedings of the International Conference on Solar Physics *"Structure and Dynamics of the Solar Corona",* ed. by B.P. Fillipov, Troitsk, Russia, October 4-8, 1999, Troitsk, p. 117 (in Russian).
Ryabov, B.I., Pilyeva, N.A., Alissandrakis, C.E., Shibasaki, K., Bogod, V.M., Garaimov, V.I., Gelfreikh, G.B.: 1999, *Solar Phys.,* **185**, 157 (Paper I).
Uralov, A.M., Grechnev, V.V, Lesovoi, S.V., Sych, R.A., Kardapolova, N.N., Treskov, T.A., Smolkov, G. Ya: 1998, *Solar Phys.,* **178**, 557.
Zheleznyakov, V.V. and Zlotnik, E.Ya. : 1964, *Soviet Astr*on., **7**, 485 .
Zheleznyakov, V.V.: 1970, *Radio Emission of the Sun and Planets*, Oxford, Pergamon Press.